

Hydrostatic pressure effects on the static magnetism in $\text{Eu}(\text{Fe}_{0.925}\text{Co}_{0.075})_2\text{As}_2$

W. T. Jin,^{1,*} J. -P. Sun,² G. Z. Ye,² Y. Xiao,³ Y. Su,¹ K. Schmalzl,⁴ S. Nandi,⁵ Z. Bukowski,⁶ Z. Guguchia,⁷ E. Feng,¹ Z. Fu,¹ and J. -G. Cheng^{2,†}

¹Jülich Centre for Neutron Science JCNS at Heinz Maier-Leibnitz Zentrum (MLZ), Forschungszentrum Jülich GmbH, Lichtenbergstraße 1, D-85747 Garching, Germany

²Beijing National Laboratory for Condensed Matter Physics and Institute of Physics, Chinese Academy of Sciences, Beijing 100190, China

³Jülich Centre for Neutron Science JCNS and Peter Grünberg Institut PGI,

JARA-FIT, Forschungszentrum Jülich GmbH, D-52425 Jülich, Germany

⁴Jülich Centre for Neutron Science JCNS at Institut Laue-Langevin (ILL),

Forschungszentrum Jülich GmbH, Boite Postale 156, 38042 Grenoble Cedex 9, France

⁵Department of Physics, Indian Institute of Technology, Kanpur 208016, India

⁶Institute of Low Temperature and Structure Research, Polish Academy of Sciences, 50-422 Wrocław, Poland

⁷Department of Physics, Columbia University, New York, NY 10027, USA

The effects of hydrostatic pressure on the static magnetism in $\text{Eu}(\text{Fe}_{0.925}\text{Co}_{0.075})_2\text{As}_2$ are investigated by complementary electrical resistivity, ac magnetic susceptibility and single-crystal neutron diffraction measurements. A specific pressure-temperature phase diagram of $\text{Eu}(\text{Fe}_{0.925}\text{Co}_{0.075})_2\text{As}_2$ is established. The structural phase transition, as well as the spin-density-wave order of Fe sublattice, is suppressed gradually with increasing pressure and disappears completely above 2.0 GPa. In contrast, the magnetic order of Eu sublattice persists over the whole investigated pressure range up to 14 GPa, yet displaying a non-monotonic variation with pressure. With the increase of the hydrostatic pressure, the magnetic state of Eu evolves from the canted antiferromagnetic structure in the ground state, via a pure ferromagnetic structure under the intermediate pressure, finally to a possible "novel" antiferromagnetic structure under the high pressure. The strong ferromagnetism of Eu coexists with the pressure-induced superconductivity around 2 GPa. The change of the magnetic state of Eu in $\text{Eu}(\text{Fe}_{0.925}\text{Co}_{0.075})_2\text{As}_2$ upon the application of hydrostatic pressure probably arises from the modification of the indirect Ruderman-Kittel-Kasuya-Yosida (RKKY) interaction between the Eu^{2+} moments tuned by external pressure.

PACS numbers:

I. INTRODUCTION

The discovery of Fe-based superconductors¹ has provided new platforms to study the intriguing interplay between superconductivity (SC) and magnetism. SC in these novel materials was found to be in close proximity to the magnetism, as it emerges when the long-range antiferromagnetic (AFM) order in the parent compounds gets well suppressed by means of chemical doping or the application of external pressure,² and the spin fluctuations are believed to be responsible for the unconventional SC in them.^{3,4}

Among various classes of Fe-based superconductors, the EuFe_2As_2 -based compounds (Eu-122) have drawn tremendous attention, as they contain two magnetic sublattices and show strong spin-charge-lattice coupling.^{5,6} In a purely ionic picture, the S -state (orbital moment $L = 0$) Eu^{2+} rare-earth ion has a $4f^7$ electronic configuration and a total electron spin $S = 7/2$, corresponding to a theoretical effective magnetic moment of $7.94 \mu_B$.⁷ EuFe_2As_2 undergoes a structural phase transition from a tetragonal to an orthorhombic phase at 190 K, accompanied by a spin-density-wave (SDW) order of the itinerant Fe moments. In addition, the localized Eu^{2+} spins order below 19 K in the A-type AFM structure (ferromagnetic layers stacked antiferromagnetically along the c axis).⁸⁻¹⁰ The undoped parent compound EuFe_2As_2 can be tuned into a superconductor by chemical substitutions into the Eu-,¹¹ Fe-,¹²⁻¹⁴ or As-site,¹⁵ respectively. The SC can also be realized by the application of external physical pressure in undoped EuFe_2As_2 with the superconducting transition tem-

perature $T_{sc} \sim 30$ K in a narrow range of 2.5-3.0 GPa.^{16?, 17}

Recently, considerable experimental efforts have been devoted to understand how the magnetism in both sublattices develops with different chemical doping.^{12,19-31} It is well established that the SDW transition of the Fe sublattice gets gradually suppressed with increasing doping level, while the magnetic order of the Eu sublattice persists over the whole doping region. The magnetic ground state of the Eu^{2+} moments displays a systematic change with increasing doping concentration, from the A-type AFM structure (with the spins lying in the ab planes) at low doping levels to the pure ferromagnetic structure (with the spins aligning along the c axis) at high doping levels.²⁴ Interestingly, the strong ferromagnetic (FM) order of the localized Eu^{2+} spins, with a huge moment close to $7 \mu_B$ per Eu, was confirmed to be compatible with the SC.^{13-15,32-36}

Nevertheless, to the best of our knowledge, only a limited number of studies about the pressure effects on the Eu magnetism in the Eu-122 compounds exist. For the undoped parent compound EuFe_2As_2 , the high-pressure ac magnetic susceptibility measurement using the piston-cylinder cell suggests that the magnetic ground state of the Eu^{2+} moments is still an AFM order in the pressure-induced superconducting phase (with the maximum applied pressure $P \sim 2.8$ GPa),¹⁷ similar to that under the ambient pressure. Further measurements using a cubic anvil cell indicate that the AFM order of the Eu^{2+} moments persists up to an applied pressure $P \sim 6$ GPa, above which it changes to the FM order, as confirmed by high-pressure x-ray magnetic circular

dichroism (XMCD) experiments.⁷ The SDW transition of Fe gets completely suppressed at the critical pressure P_C where the SC emerges. In addition, complementary high-pressure muon-spin rotation (μ SR) and magnetization measurements were performed on non-superconducting isovalent-substituted $\text{EuFe}_2(\text{As}_{0.88}\text{P}_{0.12})_2$, in which the Eu^{2+} spins were found to order in the canted AFM (C-AFM) structure in the ground state.²⁸ Possible superconducting phase (“X” phase as referred in Ref.28) was realized in $\text{EuFe}_2(\text{As}_{0.88}\text{P}_{0.12})_2$ within a very narrow pressure range of 0.36-0.5 GPa, coexisting with the magnetic order of both the Eu and Fe moments. However, the magnetic structure of Eu in the so-called “X” phase can not be unambiguously determined there.

In order to conclude how the magnetism in both sublattices develop with the external pressure and to clarify the nature of the magnetic state in possible pressure-induced superconducting phase, we have carried out complementary experiments including the electrical resistivity, ac magnetic susceptibility and neutron diffraction measurements on the $\text{Eu}(\text{Fe}_{1-x}\text{Co}_x)_2\text{As}_2$ ($x = 0.075$) single crystal under hydrostatic pressure. There are two reasons of choosing $\text{Eu}(\text{Fe}_{0.925}\text{Co}_{0.075})_2\text{As}_2$ for the high-pressure studies. Firstly, according to the established $T - x$ phase diagram of electron-doped $\text{Eu}(\text{Fe}_{1-x}\text{Co}_x)_2\text{As}_2$,²⁴ the sample with $x = 0.075$ is close to the superconducting dome. The superconducting phase might be reachable by applying moderate hydrostatic pressure. Secondly, the magnetic ground-state of the Eu sublattice in $\text{Eu}(\text{Fe}_{0.925}\text{Co}_{0.075})_2\text{As}_2$ has been determined to be a canted-AFM structure.²⁴ The Eu^{2+} spins are canted out of the ab planes with an angle of $23.8(6)^\circ$, giving rise to a net ferromagnetic moment component along the c axis. It is thus very interesting to investigate how this intermediate magnetic structure in the $T - x$ phase diagram evolves with hydrostatic pressure, and to conclude what type of magnetic order of Eu can coexist with the pressure-induced superconducting phase.

II. EXPERIMENTAL DETAILS

The single crystal of $\text{Eu}(\text{Fe}_{0.925}\text{Co}_{0.075})_2\text{As}_2$ was grown out of the Sn flux.²⁴ The concentration of Co was determined by wavelength dispersive spectroscopy (WDS). Both the ambient-pressure and high-pressure neutron diffraction experiments were performed on the thermal-neutron two-axis diffractometer D23 at the Institut Laue Langevin (Grenoble, France). A Cu (2 0 0) monochromator was chosen to produce a monochromatic neutron beam with the wavelength of 1.279 Å. For the ambient-pressure measurement, a 76 mg platelike single crystal with dimensions $\sim 6 \times 5 \times 1 \text{ mm}^3$ was mounted on a thin Al plate with a small amount of GE varnish, and put inside a standard orange cryostat. For the high-pressure measurement, a 10 mg rectangular strip with dimensions $\sim 4 \times 1 \times 1 \text{ mm}^3$ was cut from the same piece of crystal, and put inside a TiZr gasket together with some lead powders as the pressure medium. The gasket was then mounted into the VX-5 type Paris-Edinburgh pressure cell³⁷ loaded with He gas for low-temperature measurements in a 4 K dedicated cryostat. The pressure values were determined from the equation

of state of lead,³⁸ based on the lattice parameters of lead measured by neutron diffraction at a certain temperature. For both experimental conditions, the crystals were oriented with the orthorhombic b axis (or a axis due to twinning) lying vertical, so that the $(H 0 L)$ scattering plane can be accessible horizontally. (The orthorhombic notation will be used throughout this paper for convenience.)

High-pressure resistivity and ac magnetic susceptibility were measured in the Institute of Physics, Chinese Academy of Sciences, by using a self-clamped piston-cylinder cell (PCC) up to 2.2 GPa and a “Palm” cubic anvil cell (CAC) up to 14.2 GPa. The standard four-probe method was used for the resistivity measurements and the mutual induction method for the ac magnetic susceptibility measurements. The pressure inside the PCC was determined by monitoring the superconducting transition temperature of tin (Sn), which was placed together with the sample in the Teflon cell filled with the Daphne 7373 as the pressure transmitting medium (PTM). The pressure inside the CAC was calibrated at room temperature by observing the characteristic phase transitions of Bismuth (Bi). In this case, glycerol was used as the PTM.

III. EXPERIMENTAL RESULTS

Figure 1 shows the temperature dependencies of the electrical resistivity, $\rho(T)$, of the $\text{Eu}(\text{Fe}_{0.925}\text{Co}_{0.075})_2\text{As}_2$ single crystal measured with the PCC (a) and the CAC (b), respectively. At ambient pressure, an upturn in $\rho(T)$ appears at $T_S \sim 152 \text{ K}$, corresponding to the structural phase transition, as confirmed by neutron diffraction presented below. Here T_S is defined as the minimum in the first derivative of $\rho(T)$, $d\rho(T)/dT$. In addition, $\rho(T)$ shows another kink at $T_{Eu} = 17 \text{ K}$, due to the magnetic order of the Eu^{2+} moments.³⁹ With increasing pressure, T_S shifts gradually to the lower temperature, as shown in the inset of Fig. 1(a). Above 2.3 GPa, no upturn in $\rho(T)$ can be observed anymore (Fig. 1(b)), indicating that the structural and SDW transitions get completely suppressed at this pressure. However, T_{Eu} , the magnetic transition temperature of Eu, seems quite insensitive to the applied pressure and stays lower than 20 K for $P \leq 2 \text{ GPa}$. As shown in the inset of Fig. 1(b), with further increasing pressure, T_{Eu} starts to change significantly, as revealed by the non-monotonous change of the minimum in the second derivative of $\rho(T)$, $d^2\rho(T)/dT^2$. After reaching a maximum value of $\sim 52 \text{ K}$ at 6.8 GPa, T_{Eu} decreases slightly with increasing pressure, to $\sim 41 \text{ K}$ at 11.2 GPa. Interestingly, T_{Eu} reverses to increase again when more pressure is applied. At the maximum applied pressure of 14.2 GPa, T_{Eu} reaches another maximum around 49 K. It is worth noting that at 2.17 GPa, $\rho(T)$ shows a sharp drop at $T_{SC} \sim 25 \text{ K}$, suggesting the appearance of the pressure-induced SC as reported previously in the parent compound.¹⁶ The superconducting nature at 2.17 GPa is also reflected in the ac magnetic susceptibility data presented below. However, the transition to a zero-resistivity state is hindered by the magnetic order of Eu, as shown by another anomaly in $\rho(T)$ around 21 K. The pressure-induced reentrant resistivity below the superconduct-

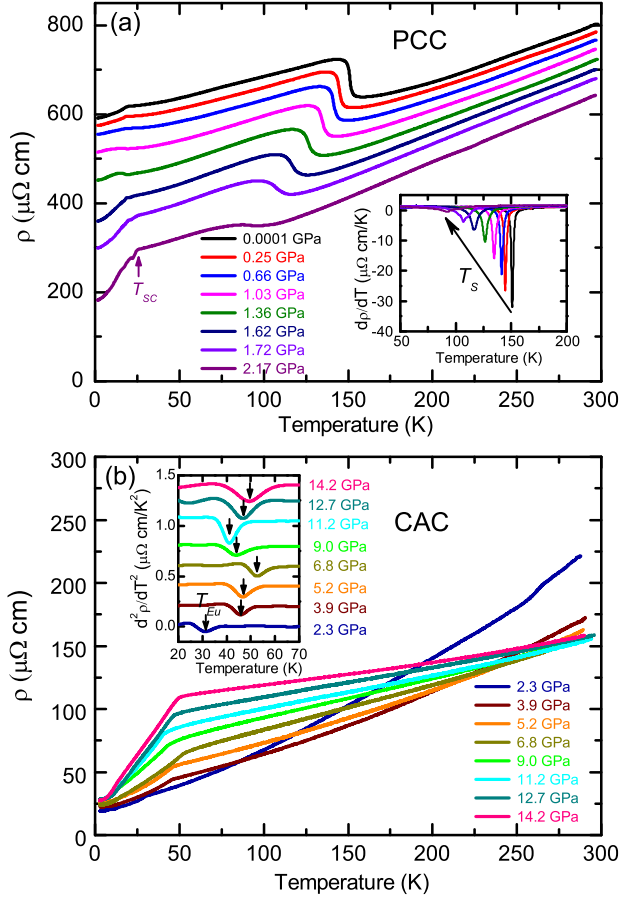


Figure 1: Temperature dependencies of the electrical resistivity (ρ) of the $\text{Eu}(\text{Fe}_{0.925}\text{Co}_{0.075})_2\text{As}_2$ single crystals measured under high pressures with the piston-cylinder cell (a) and the cubic anvil cell (b), respectively.

ing transition here resembles that observed at ambient pressure in the $\text{Eu}(\text{Fe}_{0.89}\text{Co}_{0.11})_2\text{As}_2$ single crystals grown from self-flux method,¹² ascribing to the competition between the SC and the Eu magnetic order.

The ac magnetic susceptibility of the $\text{Eu}(\text{Fe}_{0.925}\text{Co}_{0.075})_2\text{As}_2$ single crystal measured under high pressure with the PCC and the CAC is shown in Fig. 2(a) and 2(b), respectively. At ambient pressure, a peak at $T_{\text{Eu}} = 17$ K in χ' , the real part of the ac magnetic susceptibility, indicates the antiferromagnetic order of the Eu^{2+} spins. As determined from ambient-pressure neutron diffraction, the magnetic ground state of the Eu^{2+} moments is a canted AFM structure with a net FM moment component along the c axis.²⁴ With increasing pressure, T_{Eu} shifted slightly to a lower temperature for $P \leq 1.03$ GPa, as shown in Fig. 2(a), suggesting that the interlayer AFM coupling weakens under pressure. At 1.37 GPa, the antiferromagnetic peak almost gets smeared out and instead a pronounced kink is observed at $T_{\text{Eu}} = 18$ K. The kink temperature shifts continuously to a higher temperature with further increasing pressure, reaching a maximum value of ~ 52 K at 6.8 GPa

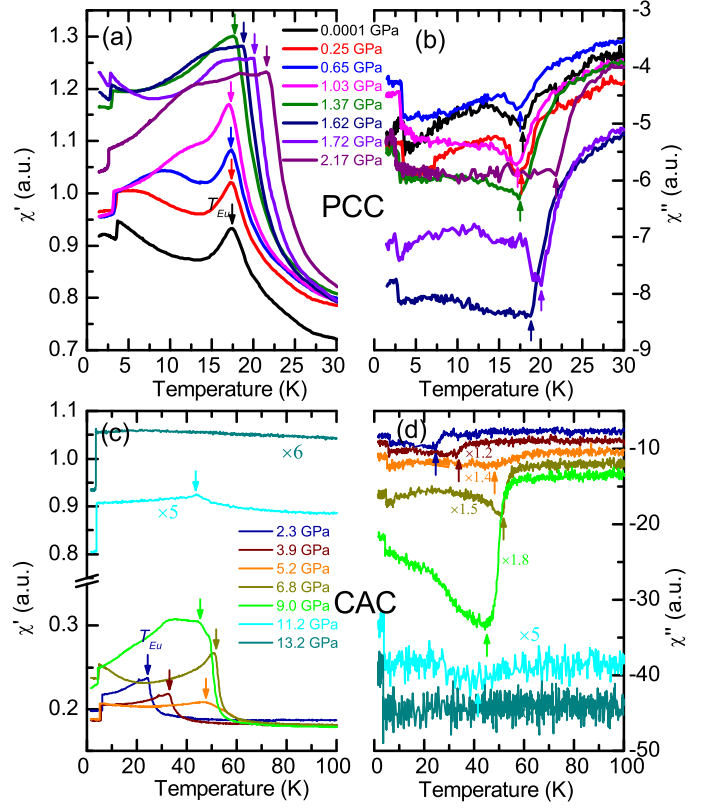


Figure 2: Temperature dependencies of the real and imaginary part of the ac magnetic susceptibility, χ' and χ'' , of the $\text{Eu}(\text{Fe}_{0.925}\text{Co}_{0.075})_2\text{As}_2$ single crystals measured under high pressures with the piston-cylinder cell (a, b) and the cubic anvil cell (c, d), respectively.

(Fig. 2(c)). The distinct tendencies of the evolution of T_{Eu} with increasing pressure for $P \leq 1.03$ GPa and $1.37 \text{ GPa} \leq P \leq 6.8$ GPa suggests that the magnetic structures of the Eu^{2+} spins might be different in the two pressure regions. With further increasing pressure ($P \geq 6.8$ GPa), T_{Eu} decreases again, as shown in Fig. 2(c), to ~ 43 K at 11.2 GPa. The pressure dependence of T_{Eu} for $\text{Eu}(\text{Fe}_{0.925}\text{Co}_{0.075})_2\text{As}_2$ obtained from the ac magnetic susceptibility measurement is well consistent with that extracted from the resistivity measurement. The anomaly at T_{Eu} can be hardly resolved in χ' for $P \geq 13.2$ GPa, implying that the Eu^{2+} moments probably order antiferromagnetically again. Furthermore, χ' shows additional features for the pressures around 2.17 GPa. Compared with other pressures, the $\chi'(T)$ curves at 2.17 GPa exhibits some diamagnetic response associated with superconductivity. As shown in Fig. 2(a), at $P = 2.17$ GPa, the slope of the $\chi'(T)$ curve shows a pronounced downward bending around 12 K, which is most likely the result of the competition between the magnetism of Eu and the pressure-induced superconductivity, as hinted by the resistivity data at this pressure value.

In order to confirm the nature of the anomalies revealed by the macroscopic measurements, the neutron diffraction mea-

measurements were performed on the $\text{Eu}(\text{Fe}_{0.925}\text{Co}_{0.075})_2\text{As}_2$ single crystal at ambient pressure and under high pressure, respectively. Figure 3(a) shows the ambient-pressure temperature dependencies of the integrated intensity of the (4 0 0) and (1 0 3) peaks, one strong nuclear reflection of the orthorhombic phase and one magnetic reflection due to the SDW order of the itinerant Fe moments, respectively. The rapid increase of the intensity of the nuclear (4 0 0) peak below $T_S = 151(1)$ K indicates the structural phase transition from a tetragonal to an orthorhombic phase, as the emergence of the orthorhombic domains has a strong impact on the extinction conditions of the nuclear Bragg reflections. The transition temperature determined here is well consistent with that determined from the resistivity measurement. In addition, fitting to the intensity of the (1 0 3) reflection for the temperature close to the transition yields the onset temperature of the SDW order of Fe, $T_{SDW} = 148(1)$ K. Compared with the parent compound EuFe_2As_2 , both transitions are significantly suppressed by 7.5% Co doping. The size of the Fe^{2+} moment is estimated to be $0.63(4) \mu_B$. Furthermore, at ambient pressure, the magnetic ground state of Eu was determined to be a canted AFM structure with a net FM moment component along the c axis, as reported in Ref. 24 and illustrated as the inset in Fig. 3(b). The Eu^{2+} spins were found to be canted with an angle of $23.8(6)^\circ$ out of the ab plane with the moment size of $6.22(3) \mu_B$. The magnetic ordering temperature of Eu was determined to be $17.0(2)$ K according to the temperature dependencies of both the (2 0 0) and (0 0 3) magnetic peaks, as shown in Fig. 3(b).

Figure 4 shows the temperature dependencies of the integrated intensity of the (4 0 0) nuclear peak measured under the high pressure at 2.0 GPa, 3.7 GPa and 6.6 GPa, respectively. Different from a rapid increase below $T_S = 151(1)$ K at ambient pressure (see Fig. 3(a)), the intensity of (4 0 0) remains almost constant for the temperature range from 15 K to 160 K when a pressure of 2.0 GPa is applied, as shown in the inset of Fig. 4, indicating the complete suppression of the structural phase transition in $\text{Eu}(\text{Fe}_{0.925}\text{Co}_{0.075})_2\text{As}_2$ under the pressure larger than 2.0 GPa ($P \geq 2.0$ GPa). This is slightly inconsistent with the result from the resistivity measurements, since an upturn can still be resolved around 92 K in $\rho(T)$ at 2.17 GPa. The discrepancy between two probes might be due to the difference in the hydrostaticity of the pressure generated by the piston-cylinder cell and the Paris-Edinburgh cell. As presented above, the signature of superconductivity is exhibited in the macroscopic measurements for the pressure close to 2.17 GPa. Therefore, the complete suppression of the structural phase transition at 2.0 GPa is in line with the expectation that the superconductivity emerges in close proximity to the criticality where the structural distortion, as well as the following or accompanying SDW order of Fe, disappears.

The effect of hydrostatic pressure on the magnetic reflections arising from the magnetic order of Eu is summarized in Figure 5. As shown in Figs. 5(a), 5(d) and 5(g), the intensity of the (2 0 0) peak always weakens significantly with increasing temperature, indicating a strong ferromagnetic contribution on this reflection, at 2.0, 3.7 and 6.6 GPa, respectively. On the other hand, the (2 0 1) reflection observed at ambient pressure due to the antiferromagnetic interlayer coupling of

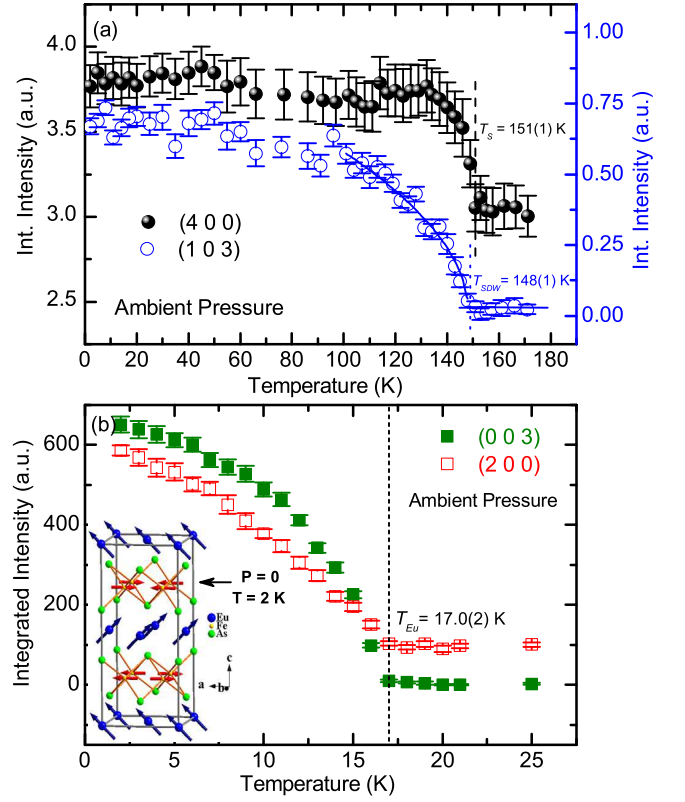


Figure 3: Temperature dependencies of the integrated intensity of the (4 0 0) and (1 0 3) reflections (a), and the (0 0 3) and (2 0 0) reflections (b), respectively, measured by neutron diffraction on the $\text{Eu}(\text{Fe}_{0.925}\text{Co}_{0.075})_2\text{As}_2$ single crystal at ambient pressure. The dash line and dot line in (a) mark the structural phase transition and the SDW transition of Fe, respectively. The short dash line in (b) marks the magnetic transition associated with the canted AFM order of the Eu^{2+} spins. The ground-state magnetic structure of $\text{Eu}(\text{Fe}_{0.925}\text{Co}_{0.075})_2\text{As}_2$ is illustrated as an inset in (b).²⁴

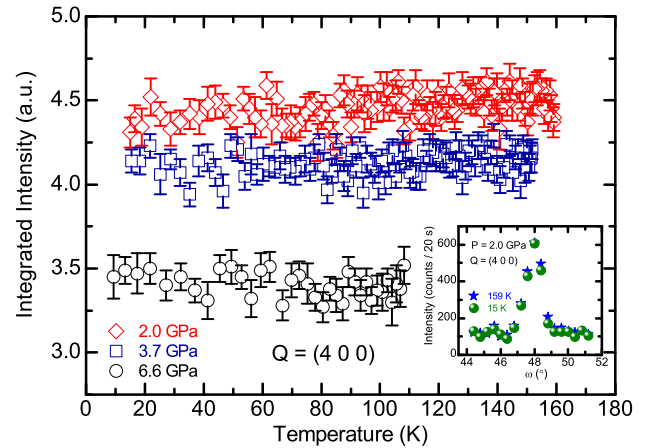


Figure 4: Temperature dependencies of the integrated intensity of the (4 0 0) nuclear reflection of the $\text{Eu}(\text{Fe}_{0.925}\text{Co}_{0.075})_2\text{As}_2$ single crystal under the high pressure at 2.0 GPa, 3.7 GPa and 6.6 GPa, respectively. The rocking scans of the (4 0 0) peak at 159 K and 15 K under the pressure at 2.0 GPa are shown in the inset.

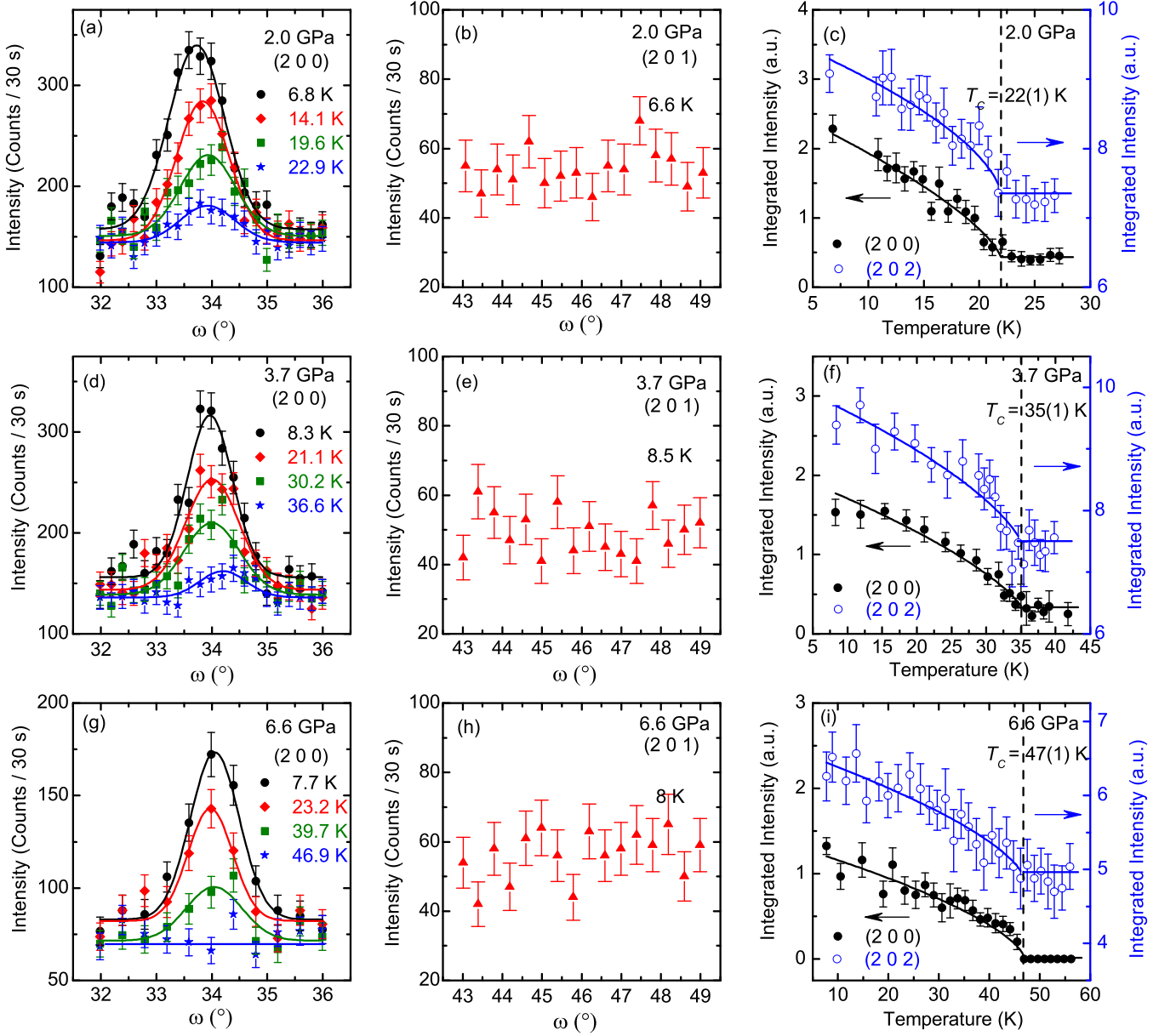


Figure 5: The summary of the neutron diffraction data on the $\text{Eu}(\text{Fe}_{0.925}\text{Co}_{0.075})_2\text{As}_2$ single crystal measured under the high pressure at 2.0 GPa (a-c), 3.7 GPa (d-f) and 6.6 GPa (g-i), respectively. The rocking scans of the $(2\ 0\ 0)$ and $(2\ 0\ 1)$ reflections at different temperatures measured at 2.0 GPa, 3.7 GPa, and 6.6 GPa are shown in (a, b), (d, e) and (g, h), respectively. The solid curves represent the fits using the Gaussian profiles. The integrated intensity of the $(2\ 0\ 0)$ and $(2\ 0\ 2)$ peaks under different pressure values are plotted as functions of the temperature in (c), (f), and (i), respectively. The vertical dashed lines mark the ferromagnetic transition temperatures of Eu at different P and the solid lines are guides to the eye.

the Eu^{2+} spins disappears upon the application of the pressure larger than 2.0 GPa (Figs. 5(b), 5(e) and 5(h)), suggesting a pure ferromagnetic order of the Eu^{2+} moments along the c axis at the applied pressure values. The temperature dependencies of the integrated intensity of both the $(2\ 0\ 0)$ and $(2\ 0\ 2)$ reflections as plotted in Figs. 5(c), 5(f) and 5(i) allow us to determine the ferromagnetic transition temperature (T_c) as 22(1), 35(1) and 47(1) K, for 2.0, 3.7 and 6.6 GPa, respectively. The observation here that T_c shifts to a higher

temperature with increasing pressure is well consistent with the results from both the resistivity and the ac magnetic susceptibility measurements within the same pressure region. It is worth noting that the net ferromagnetic contribution on the nuclear scattering part of the $(2, 0, 2)$ reflection at the lowest temperature is estimated to be around 24 % for all the three pressure values, further corroborating the ferromagnetic alignment of the Eu^{2+} moments completely along the c axis at 2.0, 3.7 and 6.6 GPa.^{24,32}

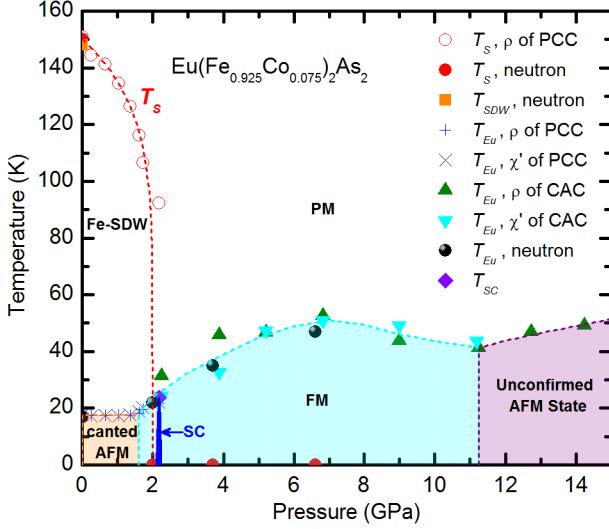


Figure 6: Pressure-temperature phase diagram of $\text{Eu}(\text{Fe}_{0.925}\text{Co}_{0.075})_2\text{As}_2$ determined from the resistivity, ac magnetic susceptibility, and neutron diffraction measurements.

IV. DISCUSSION AND CONCLUSION

Combining the results from the resistivity, ac magnetic susceptibility and neutron diffraction measurements, a phase diagram describing how the static magnetism of $\text{Eu}(\text{Fe}_{0.925}\text{Co}_{0.075})_2\text{As}_2$ develops upon the application of hydrostatic pressure is established. As shown in Fig. 6, the structural phase transition (as well as the SDW order of Fe) gets gradually suppressed with increasing pressure and disappears at a critical pressure $P_c \sim 2.0$ GPa, which is lower than $P_c \sim 2.5\text{--}2.7$ GPa in the parent compound EuFe_2As_2 ,⁷ ascribing to additional electron-doping effect from Co.

The magnetic order of Eu persists over the whole range of the applied pressure up to 14 GPa, yet displaying a non-monotonic variation with pressure. Below 1.5 GPa, T_{Eu} , the ordering temperature of the Eu^{2+} spins, stays almost constant, suggesting a canted antiferromagnetic structure with a net ferromagnetic moment component along the c direction, as observed at the ambient pressure. With further increasing pressure, T_{Eu} starts to increase, reaching a maximum value of ~ 50 K at 7 GPa. The magnetic structure of Eu in this pressure range is revealed by neutron diffraction to be a pure ferromagnetic order along the c axis. The role of the hydrostatic pressure in driving the Eu^{2+} moments to order ferromagnetically in $\text{Eu}(\text{Fe}_{0.925}\text{Co}_{0.075})_2\text{As}_2$ seems quite similar to the effect of introducing more electrons by the means of further Co doping, as reflected by the ambient-pressure phase diagram of $\text{Eu}(\text{Fe}_{1-x}\text{Co}_x)_2\text{As}_2$.²⁴ Above 7 GPa, T_{Eu} declines slightly with increasing pressure to ~ 40 K at 11.2 GPa, indicating the weakening of the ferromagnetic coupling between the Eu^{2+} moments in this pressure range. The suppression of the FM state was also observed in the parent compound EuFe_2As_2 for $P \geq 8$ GPa, which was explained as the result of the valance change from magnetic Eu^{2+} to nonmagnetic Eu^{3+} state as observed by x-ray absorption spectroscopy (XAS)

under high pressure.⁷ The pressure dependence of T_{Eu} in $\text{Eu}(\text{Fe}_{0.925}\text{Co}_{0.075})_2\text{As}_2$ for $P \leq 11$ GPa is quite similar to that in the parent compound EuFe_2As_2 ,⁷ showing an almost constant value in the AFM or canted AFM region and a dome-like variation in the FM region.

Interestingly, as revealed by the resistivity measurements, $T_{\text{Eu}}(P)$ reverses to increase again for $\text{Eu}(\text{Fe}_{0.925}\text{Co}_{0.075})_2\text{As}_2$ when more pressure is applied, which was not observed for the parent compound. As revealed by high-pressure XAS, the average valence state of Eu in both EuFe_2As_2 and EuCo_2As_2 increases with the applied pressure due to a part transition from Eu^{2+} to Eu^{3+} . However, the mean valence in them gets stabilized around +2.3 at 10 GPa and +2.25 at 12.6 GPa, for EuFe_2As_2 and EuCo_2As_2 , respectively.^{40,41} Therefore, the dip in $T_{\text{Eu}}(P)$ around 11 GPa in Fig. 6 is most likely due to combined effects of the pressure-induced valence change of Eu and the pressure-driven modification of the indirect Ruderman-Kittel-Kasuya-Yoshida (RKKY) exchange interaction in $\text{Eu}(\text{Fe}_{0.925}\text{Co}_{0.075})_2\text{As}_2$. Since the RKKY exchange coupling depends strongly on the distance between interlayer Eu^{2+} moments, which is closely related to the applied hydrostatic pressure, it is expectable that the magnetic state of Eu as well as the ordering temperature, T_{Eu} , will be tuned accordingly with increasing pressure. Unfortunately, due to the limitation of the Paris-Edinburgh pressure cell used in the neutron diffraction experiment, we can not achieve the pressure above 11 GPa so as to conclude about the nature of the magnetic state of Eu in this pressure region. The unobservable anomaly in the ac susceptibility data at 13.2 GPa as shown in Fig. 2(c) tends to support an antiferromagnetic order (either commensurate or incommensurate) of the Eu sublattice. Therefore, we refer it as an “unconfirmed AFM state” in Fig. 6. It is worth noting that a recent neutron diffraction experiment has revealed an incommensurate antiferromagnetic in-plane spiral order of the Eu^{2+} spins as the ground-state magnetic structure of Eu in EuCo_2As_2 ,⁴¹ the end member of $\text{Eu}(\text{Fe}_{1-x}\text{Co}_x)_2\text{As}_2$ system. Combining the phase diagram of the Eu magnetic ordering in $\text{Eu}(\text{Fe}_{1-x}\text{Co}_x)_2\text{As}_2$ established for the compositions with relatively lower Co concentrations ($x \leq 18\%$),²⁴ it can be concluded that with increasing Co doping level, the magnetic ground state of Eu can be tuned from the in-plane commensurate AFM order for $x = 0$, via the intermediate canted AFM structure, to a pure FM order along the c axis for $x \approx 18\%$, then probably via some intermediate complex magnetic structure, finally to the in-plane AFM spiral order for $x = 1$. Co doping drives the rotation of the Eu^{2+} moments from the ab plane to the c axis, and then from the c axis back to the ab plane. If we assume that the hydrostatic pressure plays a similar role on the FM state of Eu as the electron doping does, we might expect a “novel” magnetic state of the Eu^{2+} spins for the pressure above 11 GPa, such as an incommensurate AFM spiral order. Since we can not determine directly the nature of this possible “novel” magnetic state of Eu, we refer it as an “unconfirmed AFM state” in Fig. 6.

In addition, as hinted by the macroscopic measurements, the signature of superconductivity emerges around 2.0 GPa.

Therefore, the strong ferromagnetic order of Eu at 2.0 GPa is compatible with the pressure-induced superconductivity for $\text{Eu}(\text{Fe}_{0.925}\text{Co}_{0.075})_2\text{As}_2$, resembling the well confirmed coexistence of Eu-FM and the doping-induced SC in several families of doped EuFe_2As_2 .^{13–15,24,32–35} The pressure-induced superconducting dome of $\text{Eu}(\text{Fe}_{0.925}\text{Co}_{0.075})_2\text{As}_2$, however, is very narrow, similar to that of the parent compound EuFe_2As_2 .²

In conclusion, the effects of hydrostatic pressure on the static magnetism in $\text{Eu}(\text{Fe}_{0.925}\text{Co}_{0.075})_2\text{As}_2$ are investigated by complementary electrical resistivity, ac magnetic susceptibility and single-crystal neutron diffraction measurements. A specific pressure-temperature phase diagram of $\text{Eu}(\text{Fe}_{0.925}\text{Co}_{0.075})_2\text{As}_2$ is established. The structural phase transition, as well as the spin-density-wave order of Fe sublattice, is suppressed gradually with increasing pressure and disappears completely above 2.0 GPa. In contrast, the magnetic order of Eu sublattice persists over the whole investigated pressure range up to 14 GPa, yet displaying a non-monotonic variation with pressure. With the increase of the hydrostatic pressure, the magnetic state of Eu evolves from the canted antiferromagnetic structure in the ground state, via a pure ferromagnetic structure under the intermediate pressure, finally to a possible "novel" antiferromagnetic structure under the high pressure. The strong ferromagnetism of Eu coexists with the pressure-induced superconductivity around 2 GPa. The change of the magnetic state of Eu in

$\text{Eu}(\text{Fe}_{0.925}\text{Co}_{0.075})_2\text{As}_2$ upon the application of hydrostatic pressure probably arises from the modification of the indirect Ruderman-Kittel-Kasuya-Yosida (RKKY) interaction between the Eu^{2+} moments tuned by external pressure.

Acknowledgments

This work is partly based on experiments performed on the D23 diffractometer at the Institut Laue-Langevin (ILL), Grenoble, France. W. T. J. would like to acknowledge S. Mayr for the assistance with the cutting and orientation of the single crystal, and S. Klotz, C. Payre, E. Ressouche, W. Schmidt and T. Hansen for their help with the high-pressure neutron diffraction measurements. Z.B. acknowledges financial support from the National Science Center of Poland, Grant No. 2011/01/B/ST5/06397. JGC is supported by the National Science Foundation of China (Grant No. 11574377), the National Basic Research Program of China (Grant No. 2014CB921500), the Strategic Priority Research Program and the Key Research Program of Frontier Sciences of the Chinese Academy of Sciences (Grant Nos. XDB07020100, QYZDB-SSW-SLH013). Z. G. gratefully acknowledges the financial support by the Swiss National Science Foundation (SNF fellowship P2ZHP2-161980).

* Electronic address: w.jin@fz-juelich.de

† Electronic address: jgcheng@iphy.ac.cn

¹ Y. Kamihara, T. Watanabe, M. Hirano, and H. Hosono, *J. Am. Chem. Soc.* **130**, 3296 (2008).

² D. C. Johnston, *Adv. Phys.* **59**, 803 (2010).

³ J. Paglione, and R. L. Greene, *Nat. Phys.* **6**, 645 (2010).

⁴ P. Dai, *Rev. Mod. Phys.* **87**, 855 (2015).

⁵ Y. Xiao, Y. Su, W. Schmidt, K. Schmalzl, C. M. N. Kumar, S. Price, T. Chatterji, R. Mittal, L. J. Chang, S. Nandi, N. Kumar, S. K. Dhar, A. Thamizhavel, and Th. Brueckel, *Phys. Rev. B (R)* **81**, 220406 (2010).

⁶ Y. Xiao, Y. Su, S. Nandi, S. Price, B. Schmitz, C. M. N. Kumar, R. Mittal, T. Chatterji, N. Kumar, S. K. Dhar, A. Thamizhavel, and Th. Brueckel, *Phys. Rev. B* **85**, 094504 (2012).

⁷ R. Marchand and W. Jeitschko, *J. Solid State Chem.* **24**, 351 (1978).

⁸ S. Jiang, Y. K. Luo, Z. Ren, Z. W. Zhu, C. Wang, X. F. Xu, Q. Tao, G. H. Cao, and Z. A. Xu, *New J. Phys.* **11**, 025007 (2009).

⁹ J. Herrero-Martín, V. Scagnoli, C. Mazzoli, Y. Su, R. Mittal, Y. Xiao, Th. Brueckel, N. Kumar, S. K. Dhar, A. Thamizhavel, and L. Paolasini, *Phys. Rev. B* **80**, 134411 (2009).

¹⁰ Y. Xiao, Y. Su, M. Meven, R. Mittal, C. M. N. Kumar, T. Chatterji, S. Price, J. Persson, N. Kumar, S. K. Dhar, A. Thamizhavel, and Th. Brueckel, *Phys. Rev. B* **80**, 174424 (2009).

¹¹ H. S. Jeevan, Z. Hossain, D. Kasinathan, H. Rosner, C. Geibel, and P. Gegenwart, *Phys. Rev. B* **78**, 052502 (2008).

¹² S. Jiang, H. Xing, G. Xuan, Z. Ren, C. Wang, Z. A. Xu, and G. Cao, *Phys. Rev. B* **80**, 184514 (2009).

¹³ W. H. Jiao, Q. Tao, J. K. Bao, Y. L. Sun, C. M. Feng, Z. A. Xu, I. Nowik, I. Feiner, and G. H. Cao, *Europhys. Lett.* **95**, 67007

(2011).

¹⁴ W. H. Jiao, H. F. Zhai, J. K. Bao, Y. K. Luo, Q. Tao, C. M. Feng, Z. A. Xu, and G. H. Cao, *New J. Phys.* **15**, 113002 (2013).

¹⁵ Z. Ren, Q. Tao, S. Jiang, C. Feng, C. Wang, J. Dai, G. Cao, and Z. Xu, *Phys. Rev. Lett.* **102**, 137002 (2009).

¹⁶ C. F. Miclea, M. Nicklas, H. S. Jeevan, D. Kasinathan, Z. Hossain, H. Rosner, P. Gegenwart, C. Geibel, and F. Steglich, *Phys. Rev. B* **79**, 212509 (2009).

¹⁷ T. Terashima, M. Kimata, H. Satsukawa, A. Harada, K. Hazama, S. Uji, H. S. Suzuki, T. Matsumoto, and K. Murata, *J. Phys. Soc. Jpn.* **78**, 083701 (2009).

¹⁸ K. Matsubayashi, K. Munakata, M. Isobe, N. Katayama, K. Ohgushi, Y. Ueda, N. Kawamura, M. Mizumaki, N. Ishimatsu, M. Hedo, I. Umehara, and Y. Uwatoko, *Phys. Rev. B* **84**, 024502 (2011).

¹⁹ Anupam, P. L. Paulose, S. Ramakrishnan, and Z. Hossain, *J. Phys.: Condens. Matter* **23**, 455702 (2011).

²⁰ M. Zhang, J. J. Ying, Y. J. Yan, A. F. Wang, X. F. Wang, Z. J. Xiang, G. J. Ye, P. Cheng, X. G. Luo, J. Hu, and X. H. Chen, *Phys. Rev. B* **85**, 092503 (2012).

²¹ A. Błachowski, K. Ruebenbauer, J. Żukrowski, Z. Bukowski, K. Rogacki, P. J. W. Moll, and J. Karpinski, *Phys. Rev. B* **84**, 174503 (2011).

²² Z. Guguchia, J. Roos, A. Shengelaya, S. Katrych, Z. Bukowski, S. Weyeneth, F. Murányi, S. Strässle, A. Maisuradze, J. Karpinski, and H. Keller, *Phys. Rev. B* **83**, 144516 (2011).

²³ Z. Guguchia, S. Bosma, S. Weyeneth, A. Shengelaya, R. Puzniak, Z. Bukowski, J. Karpinski, and H. Keller, *Phys. Rev. B* **84**, 144506 (2011).

²⁴ W. T. Jin, Y. Xiao, Z. Bukowski, Y. Su, S. Nandi, A. P. Sazonov,

- M. Meven, O. Zaharko, S. Demirdis, K. Nemkovski, K. Schmalzl, Lan Maria Tran, Z. Guguchia, E. Feng, Z. Fu, and Th. Brückel, *Phys. Rev. B* **94**, 184513 (2016).
- ²⁵ G. H. Cao, S. G. Xu, Z. Ren, S. Jiang, C. M. Feng, and Z. A. Xu, *J. Phys.: Condens. Matter* **23**, 464204 (2011).
- ²⁶ H. S. Jeevan, D. Kasinathan, H. Rosner, and P. Gegenwart, *Phys. Rev. B* **83**, 054511 (2011).
- ²⁷ S. Zapf, D. Wu, L. Bogani, H. S. Jeevan, P. Gegenwart, and M. Dressel, *Phys. Rev. B (R)* **84**, 140503 (2011).
- ²⁸ Z. Guguchia, A. Shengelaya, A. Maisuradze, L. Howard, Z. Bukowski, M. Chikovani, H. Luetkens, S. Katrych, J. Karpinski, and H. Keller, *J. Supercond. Nov. Magn.* **26**, 285 (2013).
- ²⁹ S. Zapf, H. S. Jeevan, T. Ivek, F. Pfister, F. Klingert, S. Jiang, D. Wu, P. Gegenwart, R. K. Kremer, and M. Dressel, *Phys. Rev. Lett.* **110**, 237002 (2013).
- ³⁰ W. H. Jiao, J. K. Bao, Q. Tao, H. Jiang, C. M. Feng, Z. A. Xu, and G. H. Cao, *J. Phys.: Conf. Ser.* **400**, 022038 (2012).
- ³¹ W. T. Jin, Y. Xiao, Y. Su, S. Nandi, W. H. Jiao, G. Nisbet, S. Demirdis, G. H. Cao, and T. Brückel, *Phys. Rev. B* **93**, 024517 (2016).
- ³² W. T. Jin, S. Nandi, Y. Xiao, Y. Su, O. Zaharko, Z. Guguchia, Z. Bukowski, S. Price, W. H. Jiao, G. H. Cao, and Th. Brückel, *Phys. Rev. B* **88**, 214516 (2013).
- ³³ S. Nandi, W. T. Jin, Y. Xiao, Y. Su, S. Price, D. K. Shukla, J. Strempfer, H. S. Jeevan, P. Gegenwart, and Th. Brückel, *Phys. Rev. B* **89**, 014512 (2014).
- ³⁴ S. Nandi, W. T. Jin, Y. Xiao, Y. Su, S. Price, W. Schmidt, K. Schmalzl, T. Chatterji, H. S. Jeevan, P. Gegenwart, and Th. Brückel, *Phys. Rev. B* **90**, 094407 (2014).
- ³⁵ W. T. Jin, W. Li, Y. Su, S. Nandi, Y. Xiao, W. H. Jiao, M. Meven, A. P. Sazonov, E. Feng, Y. Chen, C. S. Ting, G. H. Cao, and Th. Brückel, *Phys. Rev. B* **91**, 064506 (2015).
- ³⁶ V. K. Anand, D. T. Adroja, A. Bhattacharyya, U. B. Paramanik, P. Manuel, A. D. Hillier, D. Khalyavin, and Z. Hossain, *Phys. Rev. B* **91**, 094427 (2015).
- ³⁷ S. Klotz, J. M. Besson, G. Hamel, R. J. Nelmes, J. S. Loveday, and W. G. Marshall, *High Pres. Res.* **14**, 249 (1996).
- ³⁸ T. Strässle, S. Klotz, K. Kunc, V. Pomjakushin, and J. White, *Phys. Rev. B* **90**, 014101 (2014).
- ³⁹ The ambient-pressure $\rho(T)$ curve of $\text{Eu}(\text{Fe}_{0.925}\text{Co}_{0.075})_2\text{As}_2$ in Fig. 1(a) was measured on a small strip cut from the crystal and does not show a drastic drop below 11.4 K, indicating the filamentary nature of the superconducting-like behavior observed on a much larger crystal (Fig. 1 in Ref. 24).
- ⁴⁰ L. Sun, J. Guo, G. Chen, X. Chen, X. Dong, W. Lu, C. Zhang, Z. Jiang, Y. Zou, S. Zhang, Y. Huang, Q. Wu, X. Dai, Y. Li, J. Liu, and Z. Zhao, *Phys. Rev. B* **82**, 134509 (2011).
- ⁴¹ X. Tan, G. Fabbri, D. Haskel, A. A. Yaroslavl'tsev, H. Cao, C. M. Thompson, K. Kovnir, A. P. Menushenkov, R. V. Chernikov, V. Ovidiu Garlea, and M. Shatruk, *J. Am. Chem. Soc.* **138**, 2724 (2016).